7 DISCUSSION

7.1 Test procedure

The hydrostatic pressure test was done according to BS 5480. This standard is the basis of the test procedure used by most of the manufacturers for testing of pipes and fittings. The procedure provides for easy use of measuring devices. Linear metallic strain gauges connected to quarter Wheatstone bridges were used to pick up strain variations experienced by the flanges at different targeted locations. A pressure gauge to display the internal pressure was connected to the joint assembly (See figure C.1 in appendix C).

BS 548 does not specify the failure criteria by leakage at test pressures greater than two times the design pressure of the test joint. Therefore, the leakage assessment of the joint was done in terms of ASTM F 37. This standard specifies that the results of the sealability tests must be expressed as the leakage rate of the test medium through the joints in millilitres per minute.

BS 5480 specifies that the system must be loaded up to pressures not exceeding two times the design pressure of the specimen. Furthermore, the test joint has to comply with the requirements listed in section 3.1. For the purpose of this project, the hydrostatic test facility was design such that the flanges could be tested until ultimate material failure. This allowed getting a better understanding of the different failure modes experienced by the specimens. The pressure test was performed in two stages. The first stage, which is the initial static pressure, was performed for leak tightness and damage inspection of the joint components. The second stage, which is the static pressure test, was performed in order to promote joint failure. This allowed the implementation of a safe and repeatable pressure test.

Bolts were tightened up by means of a torque wrench to ensure that the specified bolt loads were applied to the joints. The initial bolt looseness was not taken into account because there was no practical means to measure it accurately and to adjust the preload of the tightened bolts.

The maximum test pressure of all specimens was less than 10 MPa, because that was the maximum that the testing facility could apply. During testing, the hydrostatic pressure was increased at a rate not exceeding two bars per minute to avoid sudden expansion of the flange and to ensure a gentle relaxation of the gasket. Enough time was allowed for the flange to relax once the pressure load was released. This enabled capturing possible creep effects of the gasket.

The testing temperature specified by BS 5480 is 23 ±2ºC. Since the fluctuation of the testing room temperature as well as the temperature difference between the test medium and the flanges could affect the test results, specimens were conditioned at the testing temperature for about two hours immediately before the test. A calibration of instruments was done to correct possible deviations of the strain readings that might be caused by unexpected changes of the room temperature during the test.

7.2 Burn off test results

Burn off tests were performed in order to investigate the packing sequence, fibre direction, relative amount of reinforcements in the various flange laminates and to get a better understanding of the flange failure modes. The void content was not taken into account since a visual inspection of specimens showed a negligible amount of voids. Flanges were cut out into small slices as shown in figure 7.1. The average fibre contents of similar pipes and flange specimens are shown in table 7.1 and 7.2 and plotted in figure 7.2 and 7.3.

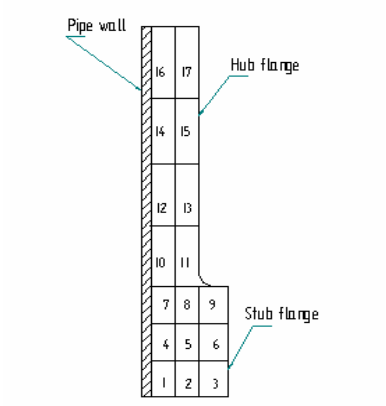

Figure 7.1: Fibre content locations along the flange

Table 7.1: Burn off test results

Location	Fibre content *Wf* (%)				
	Fabricated flanges		Amitech flanges		
	Flange 1	Flange 2	10 bar flange	16bar flange	20 bar flange
1	25.95	26.2	37.52	37.82	33.70
2	29.55	30.05	39.80	38.50	39.02
3	28.65	29.61	39.5	40.50	37.80
4	32.18	30.00	40.28	39.37	37.11
5	29.10	28.01	30.30	29.10	28.50
6	30.52	31.09	28.22	30.38	33.60
7	29.10	28.30	41.70	37.10	38.02
8	26.62	26.80	28.90	30.07	39.50
9	27.56	31.86	36.25	34.20	32.35
10	30.25	31.65	39.20	40.90	37.40
11	32.50	32.05	35.23	40.85	40.21
12	29.54	30.95	41.80	43.50	40.90
13	31.25	29.85	38.51	41.90	39.68
14	32.75	30.26	38.65	40.50	41.27
15	31.10	31.01	38.61	38.73	40.30
16	32.05	32.5	38.80	42.52	39.51
17	30.50	30.68	37.56	38.98	34.25
Average	**29.95**	**30.05**	**37.11**	**38.05**	**37.24**
Std dev	**2.00**	**1.80**	**4.16**	**4.53**	**3.56**

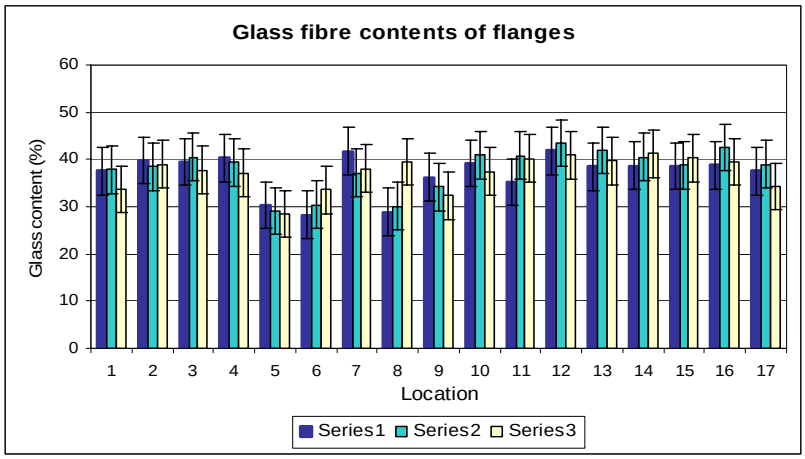

Figure 7.2: Comparison of glass fibre contents of Amitech flanges

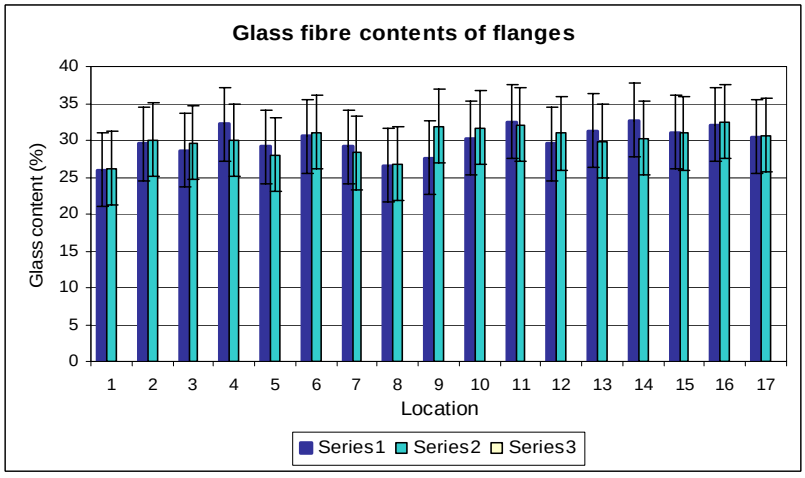

Figure 7.3: Comparison of glass fibre contents of fabricated flanges

Visual examination of the burned out specimens showed that Amitech flanges had similar reinforcement. The 20 bar flanges had lower fibre contents at locations five, six and nine. The 10 and 16 bar flanges had lower fibre contents at locations five, six and eight when compared to the rest of the flange laminate (Figure 7.2). The similarity in the patterns of the reinforcement arrangements and material distribution for the Amitech flanges indicates that the manufacturer followed the same design and manufacturing procedures. The fabricated stub flanges did not have such material distribution around the flange radius. Higher resin contents were found at locations one, five and eight. However, they did have similar patterns of material distribution

(Figure 7.4). Figure 7.4 and 7.5 show a large amount of cavities at the change in direction of fibre location and area of additional glass reinforcement insertion. High matrix contents observed at these locations are probably due to the following:

- As recommended by BS 6464, additional fibres must be inserted into the flange at the manufacturing stage to give stub thickness. Therefore, more resin is often used to prevent voids and to maintain additional glass reinforcement in the stub flange.
- Due to the large change of direction that occurs at the flange radius and the resistance of the reinforcement to bend easily through ninety degrees, CSM glass fibres tend to disperse out of the reinforcement mat and thereby cause a decrease in the fibre content. Thus a large amount of resin may be needed to avoid voids.

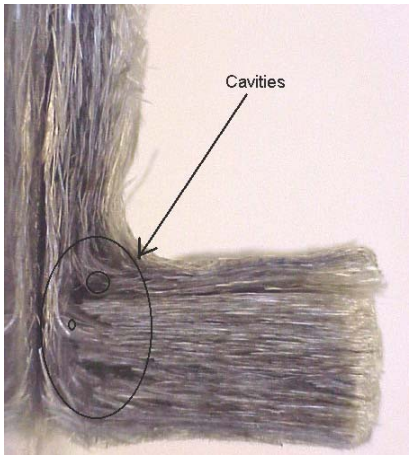

Figure 7.4: Fabricated burned out stub

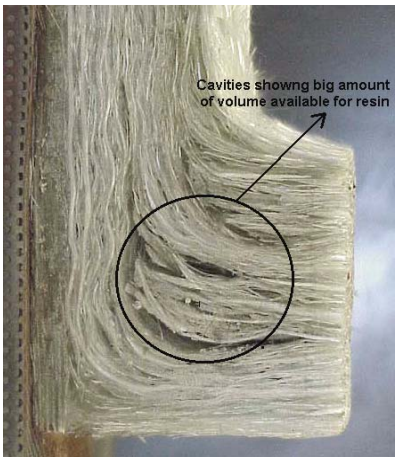

Figure 7.5: Amitech burned out stub

In general, locations 10 to 17 of all test flanges exhibited consistent and higher glass contents when compared to the rest of the flange locations. This is due to the fact that, at these locations, the hub flange has simple geometry, therefore the required glass content for the laminate can be controlled and easily achieved by the fabricator at the manufacturing stage.

From results listed in table 7.1 and plotted in figure 7.6, it can be seen that the fabricated flanges have lower fibre contents when compared to the Amitech flanges. This is probably due to the fact that they are exclusively made up of chopped strand mat reinforcement whereas Amitech flanges are fabricated using both chopped strand mat and woven roving. In general, laminates using woven roving have higher fibre contents relative to laminates using chopped strand mat [11]. Therefore, depending on the amount of woven roving layers in the laminate, GRP laminates made up of both types of reinforcement (CSM and WR) should have higher fibre content and higher in-plane strength than those exclusively made up of CSM.

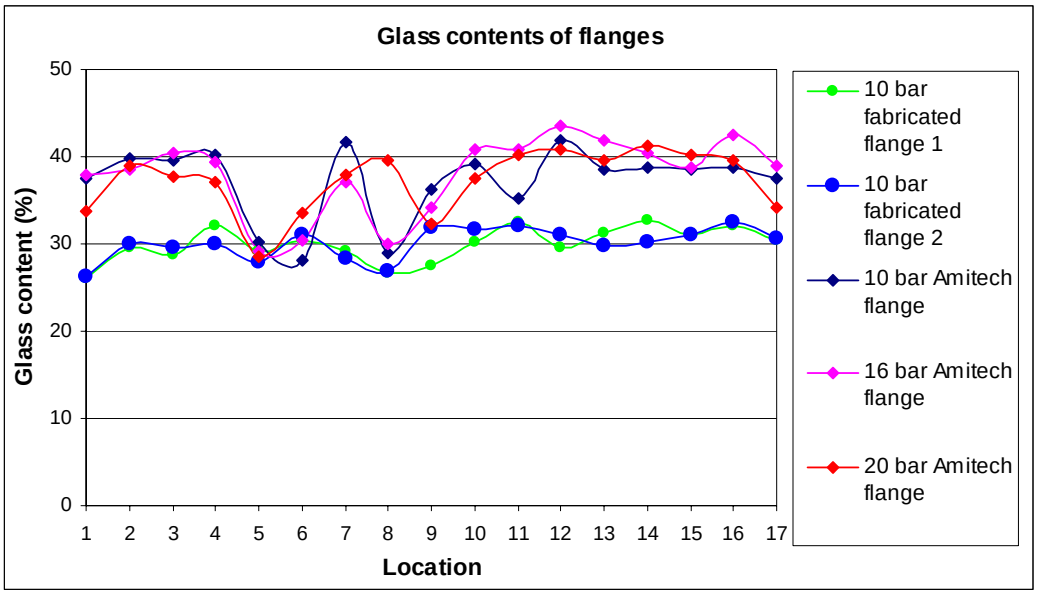

Figure 7.6: Comparison of fibre contents between Amitech and fabricated flanges

Despite the non-uniform distribution of the glass fibre content within the flange laminates, the calculated average fibre weight fractions listed in table 7.1 were in agreement with the acceptable values recommended by the different standards and technical guidelines [11, 23]. The minimum recommended glass content of flanges made by the hand lay-up method is 30 percent by mass [3, 22]. However, the difference of resin content observed between the hub and stub of the fabricated flanges might compromise to some extent the flange reliability by encouraging excessive shrinkage and generating unfavourable localized residual stress at the flange radius. This implies that effort should be done to ensure that uniform material distribution is achieved during the manufacturing stage.

Visual inspection of burn off specimens showed that Amitech pipe specimens are fibre wound constructions made up of continuous fibres laid at about ±55 degrees with respect to the axial axis. The internal corrosion barrier consists of a glass fibre corrosion resistant veil and chopped strand mat reinforcement. The pipe laminates had consistent fibre contents. The average fibre contents of the three groups of pipes were 67.57, 67.19 and 66.95 percents respectively (table 7.2). These values comply well with those specified by BS 6464. In addition, the pipe laminates had consistent fibre content. This is probably due to the fact the filament winding technique used to manufacture the pipe specimens is machine controlled.

Table 7.2: Burn off test results of Amitech pipes

Pipe	**Amitech pipes**		
	10bars flanges	**16 bars flanges**	**20bars flanges**
	***Wf* (%)**	***Wf* (%)**	***Wf* (%)**
1	68.75	67.01	68.10
2	66.28	67.37	65.80
Average	**67.52**	**67.19**	**66.95**
Std dev	**1.75**	**0.25**	**1.63**

7.3 Failure mode of flanges

7.3.1 Comparison between experimental strains at different locations

From figures 4.2 to 4.9, it can be seen that the experimental strain readings of all flanges show the same trends in both directions, although some scatter occurs at high test pressures. In terms of the strain gauge locations; the strain magnitudes experienced by different specimens increase from location one to location three. Locations one have low strains whereas locations three have high strain readings. The scatters observed among some sets of experimental readings are probably due to various reasons outlined in 4.2.

The strain variations on the flange specimens were found to be dependent on two variables, namely the flange design configuration and the clamping load acting upon the stub. At location one the thicker stub, which is intended to carry the compressive clamping load transmitted to the flange through the backing ring, acts as a rigid ring preventing the hub wall from expanding excessively in the radial direction. At location two, Amitech flanges consist of the pipe wall and hub flange, which both ensure the strength capability of the structure. The flange wall (hub) made up of chopped strand mat and woven roving reinforcement, was fabricated onto a chamfered piece of pipe. The fabricated flanges are not of the same configuration. They consist of only chopped strand mat reinforcement. Therefore, the flange strength is provided essentially by the hub wall. At location three, the structure is only composed of the pipe wall, and that provides the strength capability of the structure. In addition, this location is situated away from the constrained stub (Figure 3.5). The second factor that probably contributed to lower strain magnitudes at location one is the clamping force generated by bolt loads and transmitted through the backing ring. As the joint is assembled and all bolts tightened, the backing ring tends to compress the stub. Therefore, the compressed stub-flange is prevented from any axial and radial displacement that may be caused by the internal pressure.

7.3.2 Comparison of experimental strains at similar locations between different flanges

From the different figures shown in appendix G and H it is clear that Amitech flanges show similar behaviours at location one when tested up to four times their design pressure. The strains vary almost linearly and do not show large scatter. The axial strains experienced by the 10 bar flange (flange 1) show large scattering at test pressures greater than 5.0 MPa (Figure H.2). An excessive increase of the strain magnitude is exhibited at 7.0 MPa. The drop of the axial strain magnitude noticed at 8.00 MPa was probably due to the release of stress caused by the debonding of the pipe wall edge around the heel of the flange. In figure H.1 and H.2 it can be seen that the axial and circumferential strains exhibited by the 20 bar flanges at location one (Flange 1) are greater than those exhibited by the 10 and 16 bar flanges, whereas in figure H.3 and H.4 they seem to be smaller. These unexpected behaviours are probably due to the same factors mentioned previously in section 4.2. However, the sudden decrease of strain readings mentioned above (Figure 7.16) could also be induced by the distortion of the Wheatstone bridges, since at locations one, active strain gauges were submerged in water. The submerged strain gauge is connected to an unbalance quarter bridge, and its electrical resistance is allowed to vary slightly so that the strain variations can be captured as the test specimen compress or stretches. Assuming that the thin layer of silicon intended to seal the strain gauge terminals fails, the active gauge and water act as two resistors connected in parallel. Since the electrical resistance of tap water is very big compared to the gauge resistance ($2.5x10^5$ ohm meters at 20°C), the total electrical resistance decreases significantly. Therefore, the Wheatstone bridge experiences a drop of the output voltage, which causes a drop of the amplifier strain reading.

7.3.3 Comparison between experimental and numerical strains

Comparison between experimental and numerical strains of Amitech specimens

Experimental and numerical strain results were compared in terms of the strain gauge locations and directions at different test pressures. Numerical results of each flange model were compared to the experimental results obtained from the two actual corresponding similar flanges. In general, it was noticed that the predicted and experimental strains of Amitech flanges showed the same trend and correlated well at test pressures less than four times the operating pressures of different test specimens. The maximum percentage error between the numerical and experimental strains was found to be within 32 %. Above these test pressures, the strains results did not match well. (Figures 7.7 to 7.12). Although the material properties assigned to the model being analyzed can affect substantially the strain results, the theoretical material properties assigned to the Amitech flange models were not a major concern since they were reasonably in agreement with the results obtained experimentally (Table 5.1 and 5.2). The prediction of the material properties was carried out by applying the burn off test results to ensure that the material properties assigned to the models were relevant. Thus, the predicted strains obtained by using theoretical material properties could be trusted.

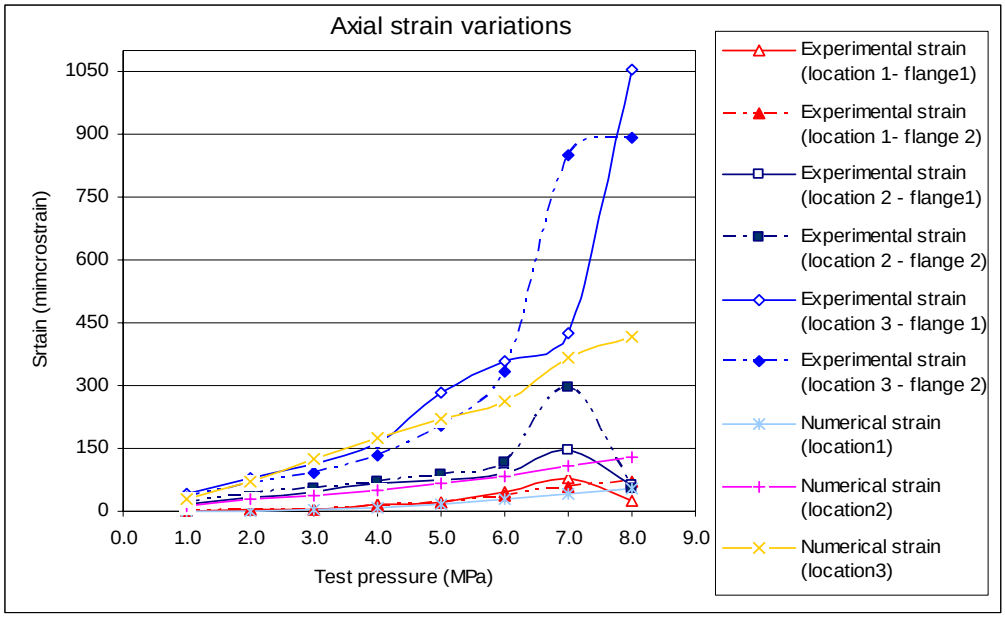

Figure 7.7: Experimental and numerical axial strains of the 10 bar flanges

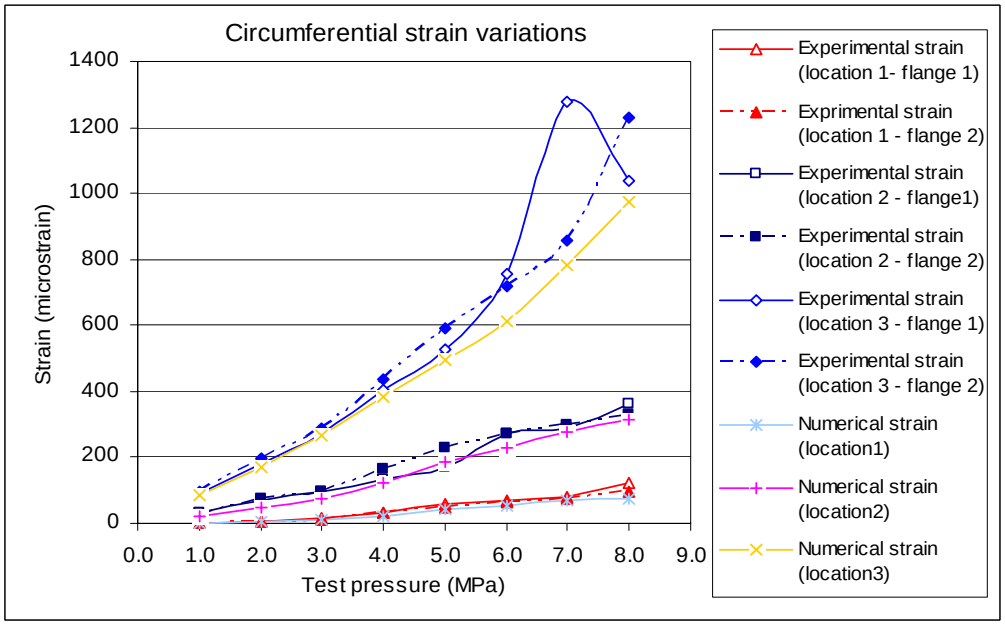

Figure 7.8: Experimental and numerical hoop strains of the 10 bar flanges

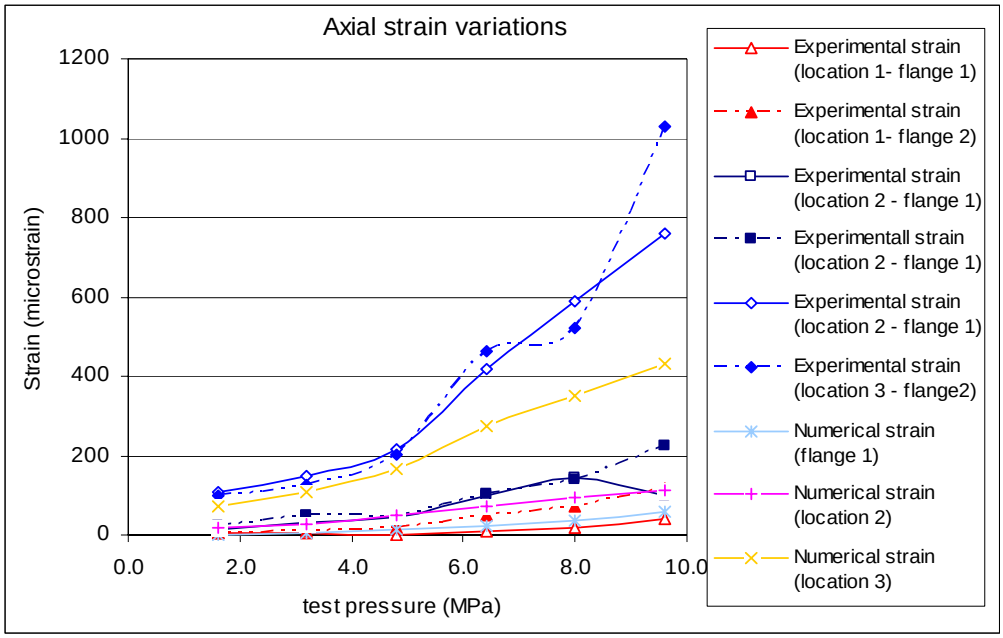

Figure 7.9: Experimental and numerical axial strains of the 16 bar flanges

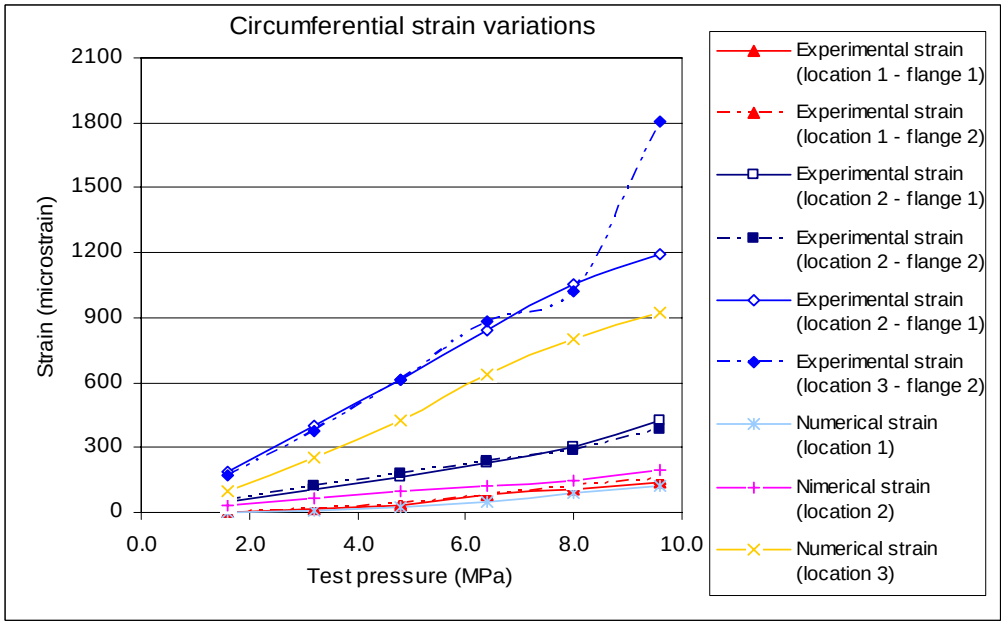

Figure 7.10: Experimental and numerical hoop strains of the 16 bar flanges

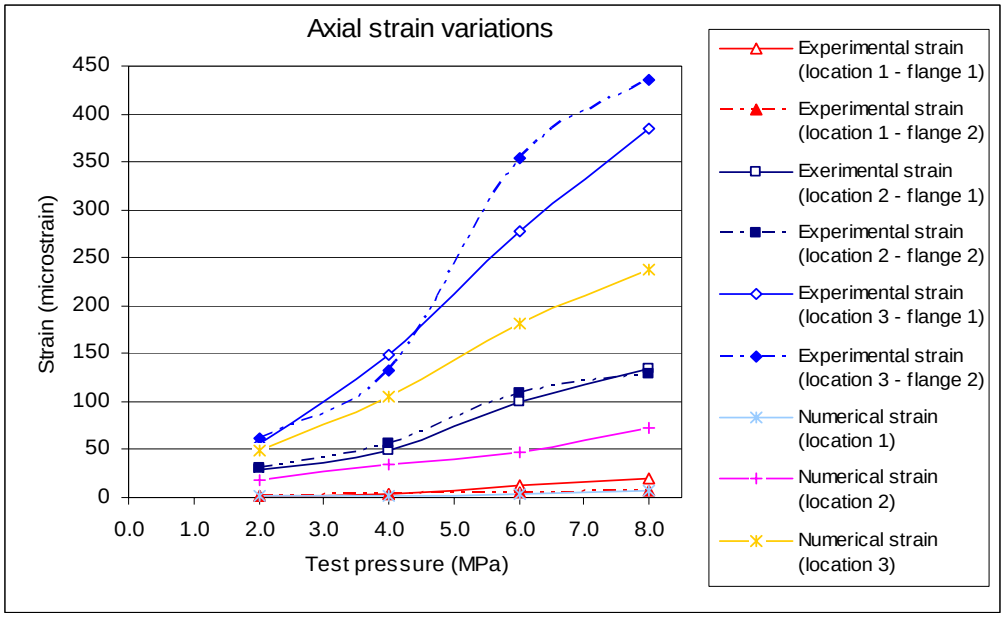

Figure 7.11: Experimental and numerical axial strains of the 20 bar flanges

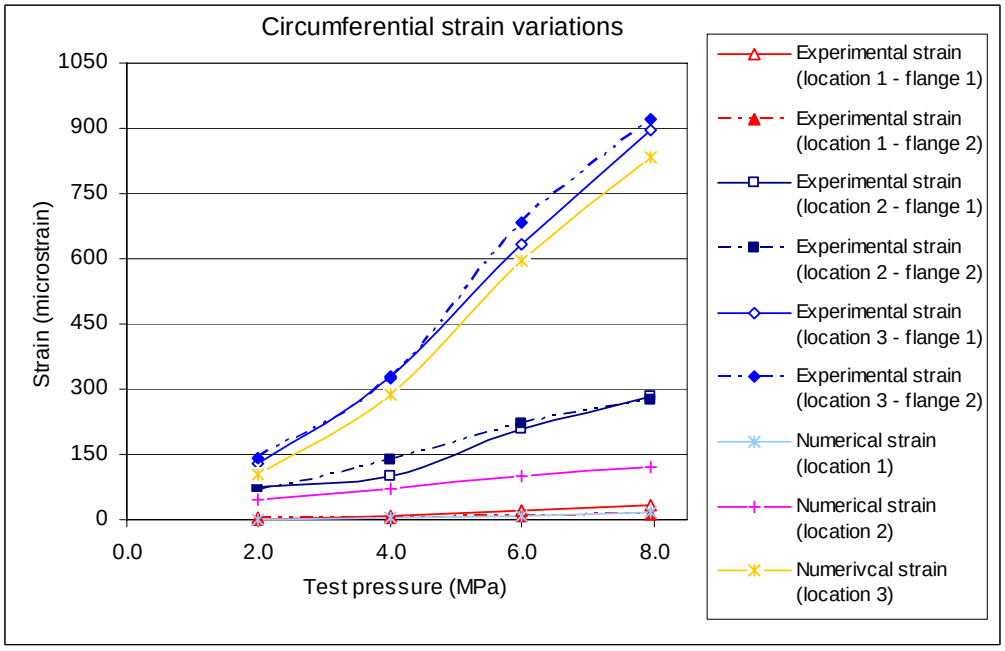

Figure 7.12: Experimental and numerical hoop strains of the 20 bar flanges

Comparison between experimental and numerical strains of fabricated specimens

Experimental and numerical results of the fabricated flanges match well in both circumferential and axial directions at test pressures less than 3.00 MPa. Above this test pressure, significant mismatch was noticed (Figure 7.13 and 7.14). A maximum percentage error of 24 % (axial strains) and 19 % (hoop strains) was noticed.

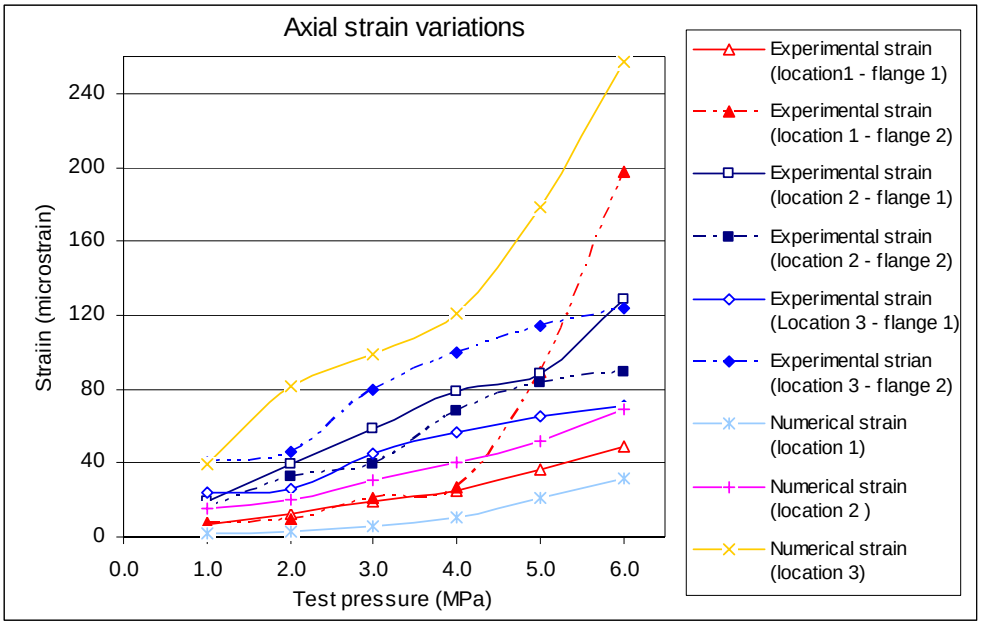

Figure 7.13: Experimental and numerical axial strains of the 10 bar flanges

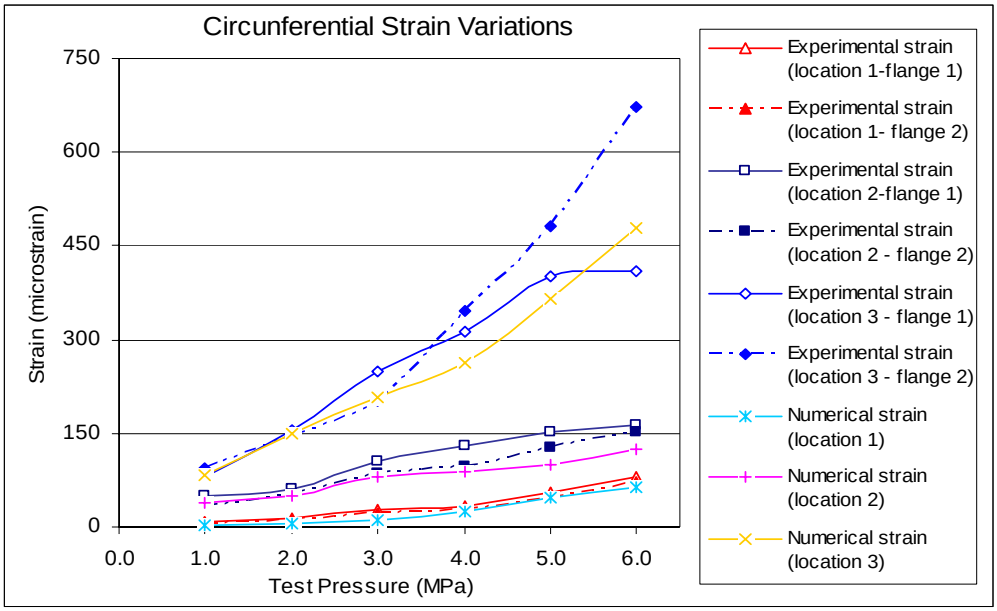

Figure 7.14: Experimental and numerical hoop strains of the 10 bar flanges

The disagreements noticed between the experimental and numerical results above 3 MPa are probably due to the non-linear behaviour of laminates. However, other factors need to be mentioned. The burn off test results indicated a non-uniform material distribution within the flange laminates whereas uniform fibre content was assigned to the flange models. In addition, the dimensions assigned to the joint models were obtained by averaging the dimensions of the two actual similar flanges. This means that the flange model did not take into account the specificities of each actual test specimen. Amitech flanges were made such that wet flanges were fabricated onto dry chamfered pipes. Since the flange joints were post-cured prior to testing, the stiffness, coefficient of thermal expansion and shrinkage mismatch between the flange and the pipe constructions might generate residual stresses on cooling [(6)]. These residual stresses could influence the flange behaviour under pressure. Cracks occurring at the gauge locations might also cause mismatch between experimental and numerical strain readings.

7.3.4 Failure mechanisms of flanges

As shown in figure 1.1, the assessment of the pipe flange was based on two aspects, namely material failure and leakage. Therefore, the experimental results discussed below include these two aspects. Analyzing the close-up views of different failed specimens illustrated in figures 7.15 to 7.21 one can notice that the ultimate material failures of test flanges are generally characterized by matrix dominated failure (pipe debonding on Amitech flanges) and fibre dominated failures extending through the flange wall around the flange radius.

Material failure of Amitech flanges

The two types of failure that are described below occurred in flange 1 at different places along the flange radius (Figure 7.15). At location one, two types of cracks are observed. Figure 7.16 shows that the failure is initiated by debonding between the pipe edge and the heel of the flange. When the system is pressurized, the axial load, which is developed by water pressure acting on the stoppers, tends to pull the pipe wall axially whereas the backing ring tends to retain the flange. This generates interfacial shear stresses between the surface contact of the pipe and hub flange. The stress analysis showed a shear stress of magnitude 25.1 MPa as the flange was loaded at 8.0 MPa (Figure 5.1). The pressure load acting on the hub flange in the radial direction generates a bending moment relative to the constrained stub. This gives rise to a peel stress at the heel of the flange. Thus, the resultant stress due to shear and peel may make the flange prone to failure by debonding. As the pressure load increases substantially, the debonding is initiated and propagates through the structure. Thus, the joint capability is compromised to some extent although the integrity of the individual component (pipe and flange laminates) remains intact. As a result, the stress is released at the edge of the pipe and the hub flange strained axially and circumferentially carries integrally the pressure load. The release of stress was indicated by the drop of the axial strain reading (at test pressure greater than 7.0 MPa) exhibited by the strain gauge positioned axially at location one (Figure 4.2). A visual inspection showed that the damage of the hub was a fibre dominated failure. The ultimate failure was characterized by breakage of the fibres (fibre pull-out) across the entire width of the hub. The damage by debonding between the pipe wall and hub

flange could be considered as a matrix dominated failure since in practice the first layers of flange construction laid upon the chamfered piece of pipe are effectively matrix bonded. The bonding between the pipe wall and hub flange might also be encouraged to some extent by the drop of joint stiffness over the test period because the pressure load was maintained for an extended period of two hours at different specified test pressures.

Figure 7.15: Failed stub flange

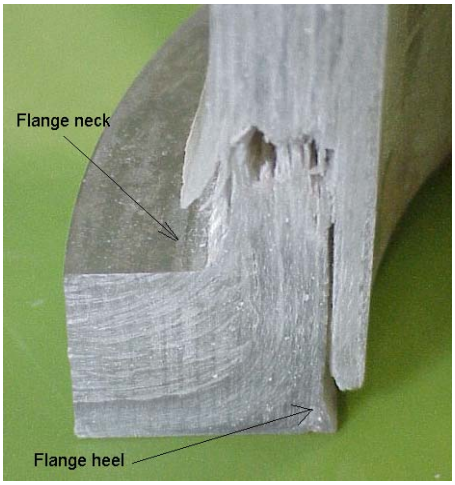

Figure 7.16: Failure by pipe debonding and stub cracks

Figure 7.18 shows a fibre dominated failure. In this case, the crack pattern is not similar to that shown in Figure 7.16. The examination of the profile view of the failed flange shows cracks extending through the flange radius. The fracture plane is inclined at about sixty degrees with respect to the radial axis of the stub. Contrarily to the failure mode depicted in figure 7.16, minor signs of pipe debonding are noticed at the flange heel. This indicates an effective interfacial bond between the pipe and hub flange around this area. The stress analysis predicted cracking that is similar to that shown in figure 7.17. Figure 5.1 and 5.4 show predicted shear (12.5 MPa) and compressive radial (20.5 MPa) stresses at the neck of the flange as the joint is loaded at 8.0 MPa. The combination of these two stresses may initiate micro-cracks over time.

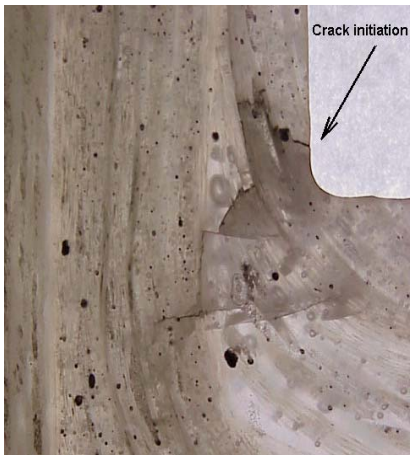

Figure 7.17: Micro crack occurrence at the flange neck

Figure 7.18: Crack extending through the flange radius

Whether failure occurs first by interfacial debonding at the heel, followed by fibre breakage across the hub width, or by cracks extending through the flange radius, dependents on various factors such as:

- localized residual stresses caused by inconsistent material distribution where change in direction of fibres occurs;
- the capability of the interfacial bond between the pipe and flange constructions;
- the uniformity of the bolt load distribution over the backing ring and the change in time of the loading conditions of the stub flange;

At location 3 the pipe wall laminate failed by leakage caused by matrix tensile cracking (Figure 7.19). No evidence of fibre breakage was noticed. The failure was characterized by the occurrence of matrix cracks parallel to the fibre direction. However, slight matrix cracks oriented transversally were noticed. Maximum in-plane shear stresses of magnitude 66.8 MPa were predicted at this location (Figure 5.1). However, the laminate was still capable of carrying the pressure load, although diffusion of water through the pipe wall occurred. The pressure gauge was found to be insensitive to the leakage rate through the pipe wall, thus the pressure load could be maintained for an extended period of time. The pipe leakage was not associated to

leakage assessment of the pipe joint since attention was focused mainly on the joint reliability. The burn off test results showed that pipe specimens supplied by Amitech were of balanced fibre wound construction, made up of continuous fibres laid at about ±55 degrees with respect to the axial axis. This type of fibre arrangement allows optimizing the strength capability of the pipe laminate by making the circumferential direction stronger than the axial direction, because the stresses due to internal pressure are greater by two times in the circumferential direction than in the axial direction [18]. Analyzing figures 4.2 and 4.3, one can notice that the axial and circumferential strains at location three vary almost linearly up to 5.0 MPa. This indicates that the laminate responded linearly to the applied load. The sudden jump of strains observed at 7.0 MPa was probably caused by the fact that matrix cracks parallel to the fibre direction occurred at the strain gauge location. Thus, the strain gauge could be stretched in an exaggerated manner and consequently cause the strain reading displayed by the amplifier to be higher than expected. Note that the axial and circumferential strain gauges were bonded respectively at about 55 and 35 degrees to the fibre directions in the global coordinate system (Figure 3.2). The drop of strains that occurred at 8.0 MPa probably indicates the release of stress caused by localized cracks occurring around the strain gauge locations.

At 6.80 MPa pressure, cracks characterized by matrix dominated failure were observed at the upper edge of the hub (Figure 7.19). This location is a region prone to stress concentration effects because of the change in laminate thickness. In addition, it has a high resin concentration (See section 7.2). One should also recognize that at the curing stage, unfavourable residual tensile stresses caused by the mismatch of material properties (stiffness and CTE's) especially in the hoop direction between the pipe and flange laminates, might occur and therefore encourage matrix crack initiation as the flange is pressurized. The stress analysis predicted shear stresses of magnitudes ranging between 25.1 MPa and 50.1 MPa at a test pressure of magnitude 8.00 MPa. Only the 10 bar Amitech flanges show this type of matrix failure.

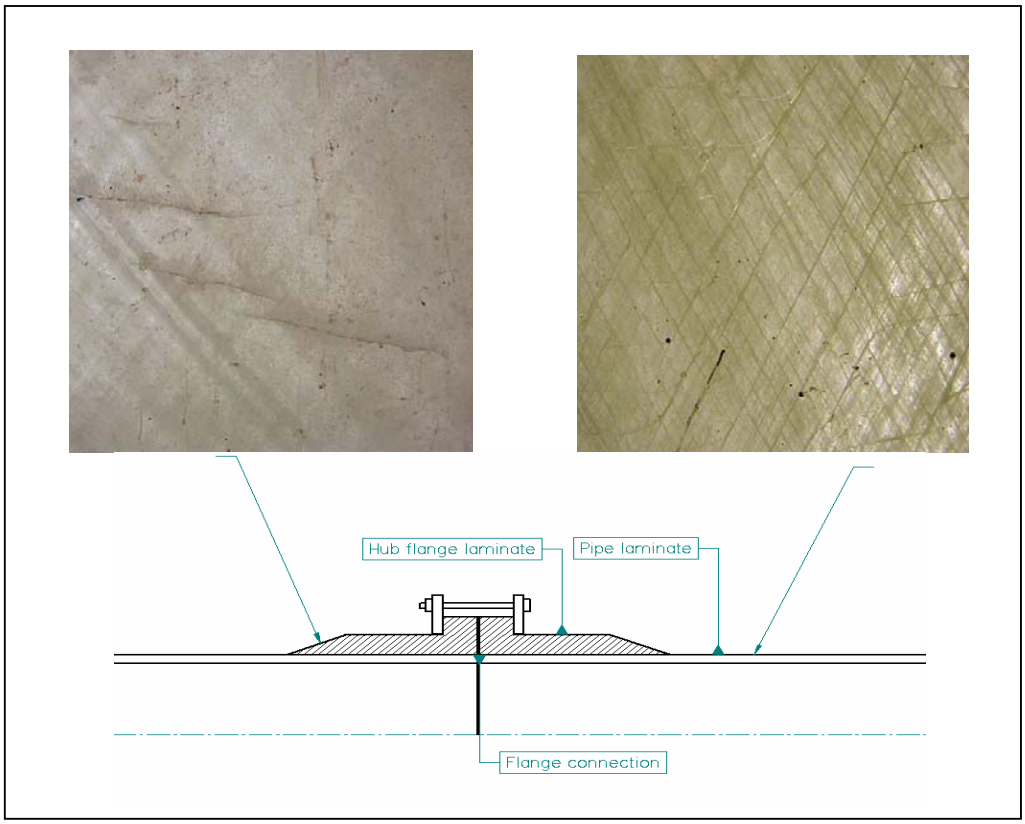

Figure 7.19: Matrix cracking location on the 10 bar Amitech flange

Material failure of fabricated flanges

The ultimate material failure of fabricated flanges was characterized by fibre dominated failure. No significant sign of matrix-dominated failure was noticed. This is probably due to the way these flanges were designed. An examination of a close-up profile view of flange 1 showed that the failure pattern was mainly characterized by crack propagations extending through the hub. At location two, fibre dominated failure characterized by cracks through the entire width of the hub and oriented transversally to the axial axis of the flange was noticed (Figure 7.20). However, the flange did not undergo similar failure all the way around the flange radius. Fibre breakage across the width of the hub at the neck of the flange and followed by slight debonding between the filler and the main wall of the hub was noticed. Cracks characterized by fibre pull-out through the main wall of the hub were observed above the heel of the flange (Figure 7.21). This difference of failure patterns is probably due to the unexpected inconsistency of the homogeneity of material distribution along the flange radius. The material inconsistency occurred probably at the manufacturing stage. A visual inspection of the butt weld and pipe construction did not show any sign of defect. The stress analysis predicted compressive radial stresses of magnitudes ranging between 17.8 and 34.2 MPa at the flange radius when the test flange was loaded at 6.6 MPa. This is not sufficient to induce material failure. However, factors such as unfavourable pre-load residual stresses due to the pull-back effect of the stub could encourage crack occurrences.

Figure 7.20: Cracks across the entire hub flange

Figure 7.21: Cracks and fibre pull-out across the flange neck

7.3.5 Evaluation of leakage

The effect of the internal pressure on the joint leak tightness needs to be discussed in order to get a better understanding of the leakage mechanism since the leakage was also considered as one of the criterion in the failure assessment of the joint assembly. The leakage assessment of test specimens was done in accordance with ASTM F 37. The test results presented in figure 7.22 show that all Amitech specimens as well as the fabricated flanges comply with BS 5480:1990 requirements at the specified maximum test pressures (See section 3.1). No sign of leakage was observed. Above these test pressures, the sealability test results were expressed as the leakage rate of the test medium through the joints in millilitres per minute.

Note that in figure 7.22 and 7.26, P stands for the rating pressure of a particular test flange.

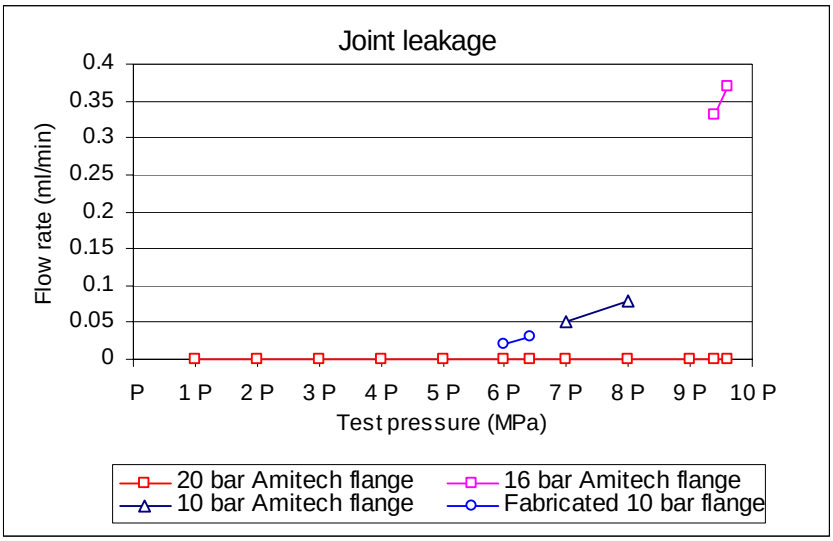

Figure 7.22 Variation of joint flow rates

Gasket blow-out was experienced by the 16 bar Amitech flanges when loaded at 9.4 MPa (Figure 7.23). The flow rate was found to be 0.33 ml/min. As the fasteners are tightened to create the required initial load and to seal the joint, the bolts elongate negligibly whereas the gasket compresses appreciably because of its low stiffness. This generates the flange pressure. The gasket, strained in compression, acts as a compressed spring that presses against the stub flanges and conforms to their face irregularities in order to ensure the leak tightness of the joint. As the test specimens are loaded to test pressures less then the critical pressure, the internal pressure load tends to separate the flanges. This implies an increase in the bolt axial load and a decrease in the clamping load between gasket and stubs. Being stiffer, the bolts elongate once again negligibly in comparison to the gasket. The small elastic stretch of the bolts does not allow the gasket to expand significantly between the stub flanges; consequently the flange pressure is still substantially preserved to maintain the seal of the joint. As the internal pressure increases, the axial load induced by the pressure load tends to separate the flanges. As a result, the compressive force holding the gasket between the stubs decreases appreciably and the gasket tends to expand in the radial direction. As the gasket contact pressure reaches a level that is less than the recommended flange pressure, the joint becomes prone to failure.

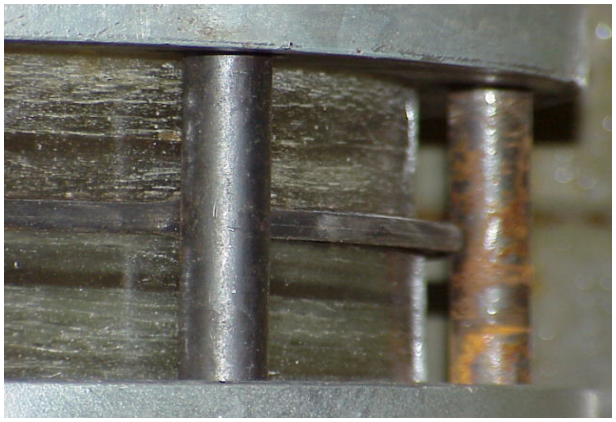

Figure 7.23: Gasket failure

7.3.6 Flange performance with respect to BS 6464

The burn off test results showed that both Amitech and fabricated flange specimens did not have uniform material distribution (Figure 7.6). The flange radius exhibited lower fibre content when compared to the hub flanges. This is because of the difficulty in ensuring a consistent material distribution in the lay-up technique, especially when the laminate has complex geometry and requires a large number of reinforcement layers. However, the average fibre contents of different test specimens complied with the minimum value recommended by BS 4994, BS 6464 and SANS 1748-2.

Visual inspection of failed test specimens showed that the fibre dominated failure took place at similar locations. Cracks extending through the laminate occurred around the flange radius. This indicates that the flange radius is the most critical part of the stub-flange. Figures 7.17, 7.18, 7.20 and 7.21 show that the failure modes exhibited by failed test flanges are generally characterized by fibre dominated failure. This indicates that the design and manufacturing specifications used in the construction of the flanges provide adequate restrictions to prevent poor material properties at the flange radius [3, 11]. However, Amitech specimens also experienced failure characterized by pipe debonding (Figure 7.15 and 7.16). This is probably due to their design and manufacturing methods. Flanges were made by applying wet layers of CSM and WR onto existing dry pipes. In addition, as the hub and pipe laminates have different material properties (stiffness and CTE's) in both axial and circumferential

directions, unfavourable induced residual stresses might occur along their interfacial bond on curing. Therefore, failure characterized by matrix failure (pipe debonding) could be expected.

The 10 bar Amitech test flanges burst at 8.6 MPa. This shows that the design specifications of Amitech specimens are in agreement with BS 6464. This standard recommends a design factor not less than eight for GRP flanges. The 10 bar fabricated flanges were designed according to BS 6464. However, they experienced the occurrence of cracks early in the test. The burst pressure (6.6 MPa) did not comply with BS 6464. This was probably due to lower and inconsistent fibre content around the flange radius (Figure 7.15). The use of chopped strand mat and woven roving reinforcements in the Amitech flanges shows that the use of both woven roving and chopped strand mat can substantially improve the reliability of the structure. A correct use of woven roving reduces the amount of reinforcement, increases the fibre content within the laminate and ensures that the in-plane properties of the laminate are fibre-dominated properties [3, 11].

7.3.7 Backing ring analysis

The flange analysis must be performed keeping in mind the behaviour of other joint components since the reliability of the joint depends on the way the clamping load is transmitted to the gasket. In practice, at the initial tightening the bolt load is transferred through the backing ring to the stub. This results in flange pressure occurring over the gasket [4]. As the test pressure increases significantly, the backing ring bends due to the axial load that tends to separate the flanges. This generates the flange pressure variation characterized by a decrease of the gasket stress between two successive bolt hole locations. Thus, substantial localized decrease of the gasket stress caused by the flange pressure variation may make the joint prone to failure by leakage. Therefore, a stress analysis has been carried out to evaluate the consequences of the bending effect experienced by the backing rings at different test pressures. This analysis was carried out to test the validity of assumptions relating to the bolt loads transmitted through the backing ring. The backing ring was modelled and meshed as a 3D isotropic model. Different values of load were applied on the upper surface of the

backing ring at the annular surface of the washer situated around each bolt hole to simulate the bolt load generated as the bolts are tightened. On the opposite side of the backing ring, the annular surface located between the inner edge of the backing ring and the bolt hole limit, was constrained for translation to simulate the interaction between the stub and the backing ring. The elastic modulus and the Poisson's ratio were 207 GPa and 0.32 respectively. A linear analysis was applied to the model and a sensitivity analysis was performed to improve the accuracy of the results. The Von Mises stress-tensor and strain magnitude plots of the 10 bar backing ring are illustrated in figure 7.24 and 7.25.

Figures 7.24 and 7.25 show that the maximum stress occurs around the bolt holes whereas the maximum strain occurs at the areas located between the bolt hole and the outer edge of the backing ring. The strain analysis showed that the strain experienced around the inner diameter of the backing ring was distributed almost uniformly. The deformation of the backing ring around its inner diameter was found to be insignificant. Furthermore, one can see that the computed stresses of different backing rings vary linearly up to the maximum test pressures of corresponding flanges (Figure 7.26). Comparing the elastic and ultimate strength of steel to the maximum computed stresses experienced by different backing rings at the maximum test pressures of flanges (table 7.3) it can be seen that the backing rings were safe from failure by yielding and fracture[(8)]. Thus, it was realistic to assume that the clamping load applied by the backing ring upon the stub flange was uniformly distributed.

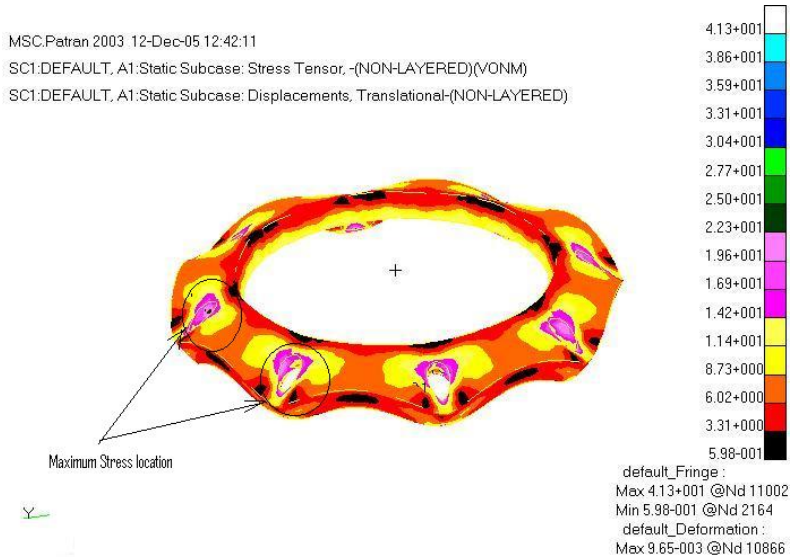

Figure 7.24: Predicted Von-Mises stresses

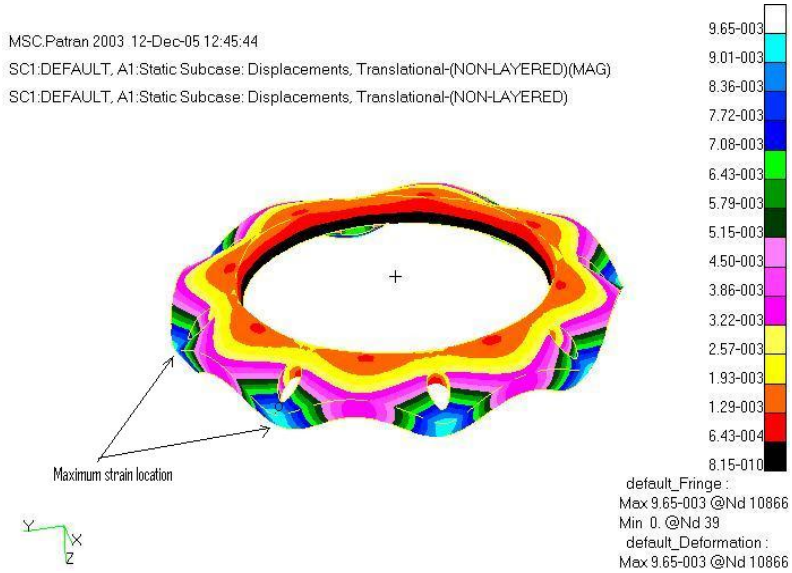

Figure 7.25: Predicted strain magnitude

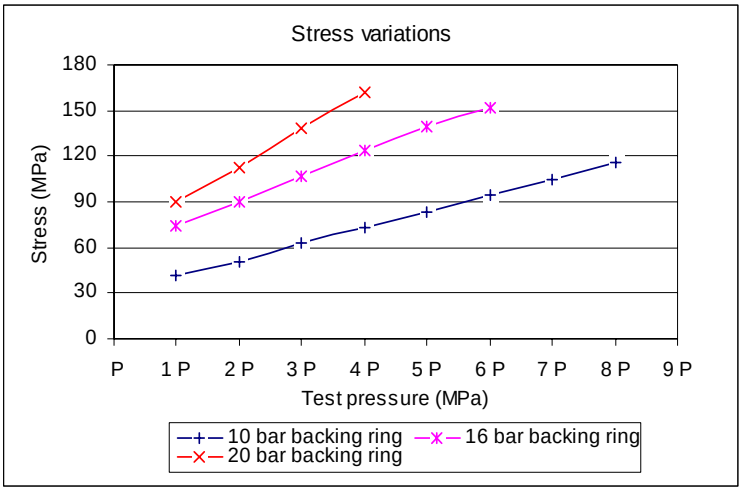

Figure 7.26: Predicted backing ring Von-Mises stresses

Table 7.3: Von Mises stresses and maximum strains

Backing ring	Max computed stress (MPa)	Max computed strain (microstrain)
10 bar backing ring	116	2.71e-02
16 bar backing ring	152	3.34e-02
20 bar backing ring	162	3.83e-02